Energy Harvesting from CO2 Emission Exploiting Ionic LiquidBased Electrochemical Capacitor

ADVANCED ENERGY & SUSTAINABILITY RESEARCH
www.advenergysustres.com

Energy Harvesting from CO_2 Emission Exploiting Ionic Liquid-Based Electrochemical Capacitor

*Davide Molino, Federico Raffone, Pietro Zaccagnini, Alessandro Pedico, Simone Martellone, Giuseppe Ferraro, Sergio Bocchini, Giancarlo Cicero, and Andrea Lamberti**

When two solutions with different compositions are mixed, the free mixing energy is released. This principle is exploited in salinity gradient power technologies like capacitive mixing (CapMix), where mixing occurs in a supercapacitor. Since this energy release holds true also for gases, research moves in the direction of harvesting energy from anthropic CO_2. To do so, it is proposed for the first time to exploit an ionic liquid (IL), both as an electrolyte and CO_2 absorbing medium in a CapMix cell. The mechanism consists in flowing a CO_2-rich gas stream, alternated to a N_2 stream, during the charging/discharging of two electrodes. The CO_2 strongly affects the electrode/IL interface and the IL physicochemical properties thereby converting the released mixing energy into electrical energy. Unlike water-based systems, where energy harvesting relies on electric double-layer expansion, we propose a new mechanism based on electrochemical potential variations during CO_2 capture/release, supported by molecular dynamics modeling. Key results include maximum voltage rise of 40 mV and energy and power densities of 40 $\mu Wh\ m^{-2}$ and 0.8 $mW\ m^{-2}$. These findings clarify the mechanism behind the electrochemical phenomena occurring when CO_2 interacts with IL and open the way to a new generation of electrochemical systems to harvest energy from CO_2 emission.

1. Introduction

The primary technologies for capturing CO_2 do not involve energy recovery. Recently, attention has shifted toward separating CO_2 from gas streams and converting it into value-added products like fuels or chemicals, driving advancements in carbon capture, utilization, and storage.[1] Existing CO_2 separation methods encompass gas scrubbing, cryogenic processes, reactions with solids, membrane techniques, and adsorption.[2] Among these, adsorption processes, notably physical and chemical absorption, have been extensively studied. Chemical absorption, involving CO_2 reacting with a solvent, offers high loading capacity even at low CO_2 partial pressures, making it suitable for low-concentration flue gas streams.[3]

Ionic liquids (ILs), low-melting salts with tunable properties, have been explored as alternative solvents due to their unique attributes like low vapor pressures and tailorability.[4,5] ILs offer opportunities for capacitive electrochemical energy storage devices, complementing battery and supercapacitor technologies.[6,7] While rechargeable batteries provide high energy capacity, supercapacitors excel in power and cycle life.[8,9] ILs have been used as electrolytes in supercapacitors, mitigating solvation effects and enhancing capacitance.[10,11]

Capacitive mixing (CapMix) technology, derived from supercapacitor principles, harnesses energy from salinity gradients.[12] The energy gain is achieved when an electric double layer (EDL) forms due to ion adsorption, expanding in low ion concentrations and increasing the voltage difference between electrodes. More recently, modified CapMix cells have employed CO_2 reactions to create ion concentration differences, facilitating energy harvesting.[13,14]

Hamelers et al. proposed a modified CapMix cell in which a membrane electrode assembly (MEA) aqueous solution reacts with CO_2 to produce carbonic acid that self-dissociates into protons (H^+) and bicarbonate ions (HCO_3^-).[13] The resulting difference in the ion concentration between the air-flushed solution and the CO_2-flushed solution can be used to gain electrical energy. In 2017, Kim et al.[14] further improved this concept by proposing the exploitation of the pH gradient between two

D. Molino, F. Raffone, P. Zaccagnini, A. Pedico, S. Martellone, G. Ferraro, S. Bocchini, G. Cicero, A. Lamberti
Dipartimento di Scienza Applicata e Tecnologia (DISAT)
Politecnico di Torino
Corso Duca Degli Abruzzi, 24, 10129 Torino, Italy
E-mail: andrea.lamberti@polito.it

P. Zaccagnini, S. Martellone, G. Ferraro, S. Bocchini, A. Lamberti
Center for Sustainable Future Technologies (CSFT)
Istituto Italiano di Tecnologia
Via Livorno 60, 10144 Torino, Italy

A. Pedico
INRiM - Istituto Nazionale di Ricerca Metrologica
Str. delle Cacce, 91, 10135 Torino, Italy

The ORCID identification number(s) for the author(s) of this article can be found under https://doi.org/10.1002/aesr.202500019.

DOI: 10.1002/aesr.202500019

aqueous solutions by sparging 1 M $NaHCO_3$ with either air (pH 9.4) or CO_2 (pH 7.7). In this case, MnO_2-based electrodes are used as pH-sensitive materials, able to generate a voltage difference of 196 mV between the two electrodes.

Several points are critical in both these processes: first, the choice of an aqueous-based solution to trap the CO_2. It is important to recall that aqueous amine scrubbing technology (such as MEA-based system) is currently considered the most mature technology that can be used to capture CO_2 from postcombustion gases due to its stable operation, good reactivity, and high absorption capacity. However, the capture of CO_2 with MEA involved chemical absorption with associated high enthalpy values. The high cost also causes this process to be unattractive for large-scale operations. Besides the energy penalty, the MEA-based systems suffer several other drawbacks such as high volatility, tendency to degradation (above 393 K), and equipment corrosion. These drawbacks cause solvent loss and contamination of the environment. Apart from the limitation intrinsically present in this solution, from the point of view of the CO_2 absorption there are also several constraints on the electrochemical side. An additional limitation comes from the whole working mechanism that results in a highly diluted CO_2 stream, useless for its valorization in added value products (e.g., fuels, chemicals, materials, etc.) based on the circular economy principle.

Here, we proposed for the first time the exploitation of an IL into a CO_2-based capacitive mixing system revolutionizing the working mechanism of the technology itself.

Indeed, by moving from an aqueous-based electrolyte toward an IL, we observed a different behavior of the electrochemical cell that can be only explained by a different working mechanism with respect to the previously proposed EDL expansion.[12–14] Coupling the experimental activity with the modeling allowed us to predict, validate, and guide the investigation, clarifying the mechanism behind the behavior of ILs used in the presence of a CO_2 stream in an electrochemical system (the implemented system is visible in **Figure 1**a). The attention was devoted to the main phenomena involving the different potentials at the electrode/electrolyte interfaces and the "bulk"-interface between imidazole carbamate and pure imidazole in the IL-electrolyte.

2. CO_2 Capacitive Mixing (CO_2CAP)

As preliminary measures, it was decided to perform some absorption tests on the 1,8-Diazabicyclo[5.4.0]undecanium Imidazolide IL [DBUH][Im]. According to Table S1, Supporting Information, [DBUH][Im] shows an increase of weight of about 15.7% that corresponds to the adsorption of 1 mole of CO_2 for each mole of ILs as already reported in the literature.[15] The mechanism proposed was reported in Figure 1b. According to experiments,[16,17] the process of CO_2 capture from [DBUH][Im] takes place at the anion. One of the two negatively charged nitrogen atoms interacts with the carbon atom of CO_2 forming carbamate. Instead, the high basicity of DBU negates the reaction with CO_2. Consequently, the cation remains unchanged during the absorption process, as confirmed by density functional theory simulations.[18] Such a mechanism allows for up to 1:1 CO_2/IL mol capture.

Figure 2a shows the infrared analyses of [DBUH][Im] before and after CO_2 adsorption, it should be underlined that the infrared spectrum of the [DBUH][ImCO_2] contains a new peak near 1700 cm^{-1}, which could be attributed to a carbamate (C═O) stretch, however, it is also interesting to underline that the stretching at 1607 cm^{-1}probably due to the $[Im]^-$ stretching is splitting into two different signals at 1640 and 1590 cm^{-1}, this is clearly visible in other works (e.g., Figure 8 of ref. [15]) but not commented.

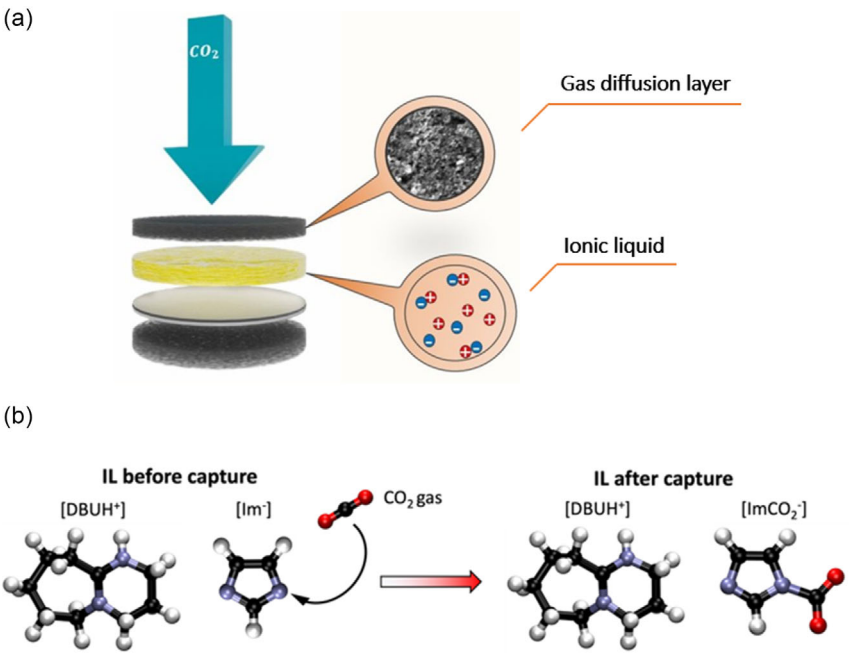

Figure 1. a) Schematic of the electrochemical cell, b) CO_2 absorption mechanism by [DBUH][Im].

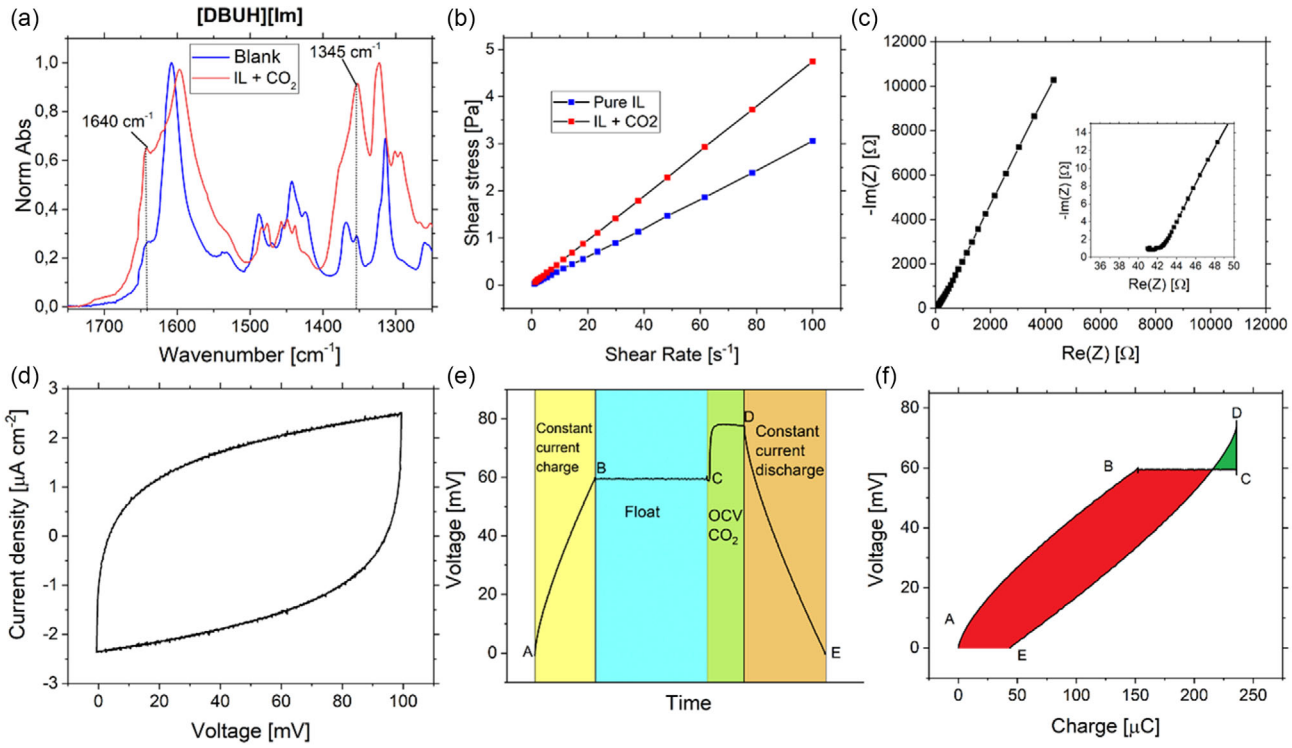

Figure 2. a) Infrared spectra of [DBUH][Im] before (black), after the absorption of CO_2 (red), b) viscosity variation due to CO_2 capture, and c) EIS GDL|[DBUH][Im]|GDL. d) cyclic voltammetry (CV) of GDL|[DBUH][Im]|GDL, e) CapMix procedure with pure [DBUH][Im], and f) the related V versus Q energy space highlights the inefficient harvesting process if exploiting the complete voltage window. The red shaded area represents the unrecovered energy while the green one highlights the voltage range at which energy can be recovered. For both graphs, the AB stage is the constant current charging at 1 μA cm^{-2}, BC the floating period, CD the CO_2 flushing stage, and finally, DE the discharging phase at 1 μA cm^{-2}.

Viscosity measurements were conducted on the [DBUH][Im] before and after the absorption of CO_2 (Figure 2b). The [DBUH][Im] was taken out from the glovebox and then immediately analyzed, while the [DBUH][ImCO_2] was sparged for 60 min with a 50 mL min^{-1} constant flux of CO_2. Both samples were then subjected to a continuous mode analysis applying an increasing shear rate from 1 to 100 s^{-1}. It is possible to notice the Newtonian behavior of both samples. Moreover, evaluating the viscosity, it is possible to notice how its value doubles: from 30.3 mPa s for pure IL to 60.5 mPa s for the [DBUH][ImCO_2].

The first device tested is composed of two circular gas-diffusion layer (GDL) electrodes (d = 18 mm) and 150 μl of [DBUH][Im]. Before performing the CapMix cycle, the electrochemical performances of the device were tested by exploiting impedance spectroscopy (Figure 2c) and cyclic voltammetry between 0 V and 100 mV (Figure 2d). From these measurements, it was possible to evaluate an equivalent series resistance equal to about 40 Ω, and a capacitance equal to 0.2 mF cm^{-2}.

The very first attempts were based on CapMix procedures from Brogioli.[12] In this scenario, the adopted protocol, depicted in Figure 2e, consists of a 4-step procedure: 1) a constant current charge to a floating voltage is used to store charges at the interface of the electrodes; 2) flush of CO_2 (50 mL min^{-1}) inside the device in open circuit conditions until reaching a peak in the voltage; 3) stop to flux the gas and discharge the gained voltage on an external load through a constant current (equal in modulus to the one used to charge up to the floating voltage); and 4) flush of N_2 (50 mL min^{-1}) inside the device to remove the CO_2 and get back to the initial conditions.

Prior to CapMix measurements, the electrochemical stability window of the system GDL|[DBUH][Im] was analyzed to evaluate the polarization limits avoiding electrolysis. We found poor anodic stability of the IL due to possible degradation of the imidazole ion (see Figure S11, Supporting Information). For this reason, all the successive experiments were performed by analyzing reduced polarization windows otherwise a huge electrode unbalanced geometrical area would have been necessary to exploit the full cation potential window. According to our results, to exploit the 1.1 V voltage window of the electrolyte, the electrodes' area ratio should be 2:1. However, since the self-discharge is greater at high voltages, we found that it can be convenient to work also with symmetrical electrodes at reduced voltage. Hence, in the CapMix measurements, the floating voltage was set to 60 mV since at this value the self-discharge was the minimum detected with symmetrical electrodes. It was decided to hold this voltage for 5 min to ensure a correct accumulation of the charges at the electrode interface. To charge and discharge the device, the current was set at 1 μA cm^{-2}.

From the CapMix cycle reported in Figure 2e, it is possible to observe the voltage rise due to the absorption of CO_2 in the electrolyte. The drawback is related to the energy balance: exploiting this protocol, the energy recovered is much smaller than the energy used to charge up the device.

In the V versus Q plot, AB segment represents the charging step, BC is related to the float period, CD is the voltage rise due to the CO_2 capture, and DE is the discharging process. From this graph, the green shaded area (proportional to the recovered energy) is much smaller than the energy spent to polarize the device, because of the energy spent holding the device at a fixed voltage. For this reason, the floating step was removed to minimize the energy spent to charge the device prior to CO_2 absorption, however, the energy balance remained still negative (see Figure S13, Supporting Information).

The problem can be explained starting from the input energy efficiency of the bare device and its self-discharge behavior without CO_2 absorption events. As reported in Figure S11b, Supporting Information, the galvanostatic profile of the bare device suggests a low energy efficiency, quantified to be 65%.

The nonlinear V(Q) relationship does not allow to quantify a constant device capacitance ($1/C = dV/dQ$) as for the CapMix processes investigated in aqueous solutions. Moreover, due to the presence of a chemical reaction, it is also not possible to fully address the voltage variation to a pure electrostatic phenomenon since a difference in activity coefficients can be detected as a measurable electric potential variation, hence voltage variation.[19] Because of these reasons, further investigation was carried out by exploiting molecular dynamics simulations to determine the mechanism and its eventual differences from the pure electrostatic CapMix.[20]

The nonlinear V(Q) relationship can be ascribed to a nonideal interfacial behavior usually attributed to surface roughness, ion adsorption, and surface tension which cause increased dissipative behavior,[21,22] hence, providing self-discharge and reducing the energy efficiency. To prove this, we diluted the IL in an organic solvent to improve the interfacial properties and reduce the repulsive behavior of the ionic charges by increasing the electrolyte permittivity. The selected solvent was propylene carbonate (PC), chemically compatible with the IL. Further, classical molecular dynamics simulations were implemented to unravel the nature of the energy harvesting process.

3. Modeling of the Phenomenon Observed

To understand the mechanism that determines the voltage rise when CO_2 is fluxed in, we performed classical molecular dynamics simulations of the device. First, we investigated the carbon electrode/IL interface for different degrees of CO_2 capture.

We explored pristine [DBUH][Im], a mixture of 50% of [DBUH][Im] and 50% of [DBUH][$ImCO_2$], and the fully saturated [DBUH][$ImCO_2$], describing different stages of the capture process. In **Figure 3**a, comparison of the electric potential profile at the interface is shown for the three IL mixtures. As the amount of CO_2 increases, the difference between the potential at the electrode and the one at the bulk progressively reduced down to the point where, for complete saturation of the [Im] anions, the electrode potential lies under the bulk potential of the IL.

By looking at the ion distribution (Figure 3b), it is noticeable the lack of a significant expansion of the double layer as in all three distributions the oscillating pattern ceases at 1.6 nm from the surface. This is a striking difference compared to the CapMix technology where the change in capacity that allows for energy extraction is mainly attributed to the variation in extension of the double layer between a solution containing a low concentration of ions and a solution containing a high ionic concentration. The mechanism of voltage variation, that in the present device allows for the energy harvesting, must then lie in a different aspect of the interface.

We notice that most of the potential drop, that determines the different behavior of the three electrolytes, takes mainly place within the first few Angstroms from the interface. Such variation is caused by the surface dipole created by the closest charge layers. By inspecting the molecule orientation at the interface in the two extreme cases, no and full CO_2 capture, we can understand the origin of the different potential variations at the interface (see Supporting Information for the angular distribution of the ions as a function of the distance). While the cation in both cases conserves the same orientation, i.e., it lies flat on top of the carbon electrode, the anions change considerably their orientation before and after capturing CO_2. [Im] is found to stay perpendicular to the electrode surface, directing its negatively charged nitrogen atoms away from the electrode. Such orientation was explained in terms of minimization of the interface energy. The negative charge in [Im] is mainly localized on one side of the molecule, next to the N atoms. As discussed in ref. [23], this causes the molecule to point the charged center toward the bulk of the IL where the other charges are located and away from the electrode surface. The opposite side, characterized by carbon atoms, shows affinity with the electrode material and,

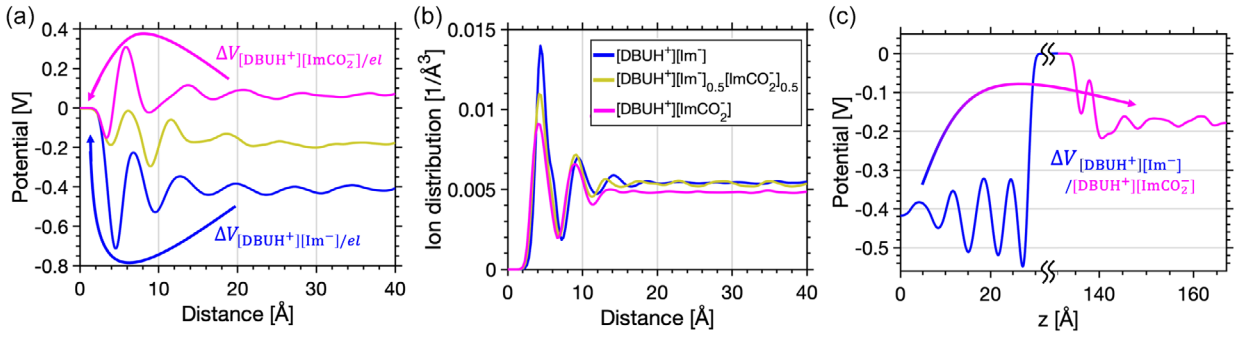

Figure 3. a) Electric potential and b) ion distribution as function of the distance from the electrode for [DBUH][Im], [DBUH][$ImCO_2$], and [DBUH][Im]$_{0.5}$[$ImCO_2$]$_{0.5}$, respectively in blue, magenta, and ochre. c) Bulk potential level differences between [DBUH][Im] and [DBUH][$ImCO_2$].

consequently, it is found in contact with the surface.[23] Accordingly, as shown in the Supporting Information, both the positively charged [DBUH] nitrogen atoms and the neutral [Im] carbon atoms are found to belong to the first layer at the interface with the electrode, whereas the negative [Im] nitrogen atoms are mainly found in the second layer. Such cation–anion configuration (see the overall ion distribution in the Supporting Information) leads to a strong surface dipole that causes the potential drop, $\Delta V_{[DBUH^+][Im^-]/el}$, at the electrode/[DBUH][Im] interface seen in Figure 3a. [$ImCO_2$], on the contrary, rather stays flat on the surface. The chemisorption of CO_2 contributes to the redistribution of charge within the imidazole molecule. Compared to [Im], the charge in [$ImCO_2$] is more evenly spread as shown in the Supporting Information. As previously reported,[23] this is likely to cause the molecule to remain flat on the electrode due to a lack of preferential direction for the anion to orient when interacting with the nearby counterions. In facts, the [DBUH] nitrogen and the [$ImCO_2$] nitrogen and oxygen atoms are found to be belong to the first layer (see Supporting Information). As both [DBUH] and [$ImCO_2$] are flat at the surface (see the plot of the ion distribution at the interface in the Supporting Information), the resulting surface dipole is minimal. The $\Delta V_{[DBUH^+][ImCO_2^-]/el}$ is then, accordingly, small. So, a first effect, that can explain the potential variation when CO_2 is flux in, is identified: a change of the orientation of the ions at the interface.

The electrode/IL interfaces are not the only interfaces characterizing the proposed device. Because CO_2 is absorbed in the IL only on one side of the device (from the permeable electrode side), an additional interface forms where the reacted [DBUH][$ImCO_2$] meets the pristine [DBUH][Im]. The two ILs are likely to have different bulk levels that determine a potential drop, $\Delta V_{[DBUH^+][Im^-]/[DBUH^+][ImCO_2^-]}$, within the electrolyte. Because the interface is given by the diffusion of [$ImCO_2$] ions, it is not as marked as the one found between electrode and IL. However, regardless of the sharpness of the interface and its potential function, what contributes to the measured voltage is ultimately the difference in the bulk potential levels of the two ILs. We then focused on calculating the bulk levels by simulating the two distinct ILs separated by a large vacuum layer. Figure 3c shows the difference in bulk levels. [$DBUH^+$][$ImCO_2^-$] is found to have a slightly higher potential level than [$DBUH^+$][Im^-]. The ion density is contextually different. [$DBUH^+$][$ImCO_2^-$] is, indeed, characterized by a smaller ion density compared to [$DBUH^+$][Im^-] due to the presence of CO_2 that increases the spacing among ions (see Supporting Information). The formation of a bulk potential level difference due to the nature of the two ILs is, then, the second effect that, along with the ion reorientation, can give rise to the measured potential variation induced by the CO_2.

Based on the simulations, we can propose a new mechanism for energy harvesting that describes the process of energy harvesting from CO_2 capture. At the beginning of the operation, only the pure IL [DBUH][Im] is present. If no external voltage is applied the two interfaces are symmetrical. The potential drops at the two ends cancel out so the overall measured voltage is equal 0 V and no charge redistribution takes place (see **Figure 4**a). The circuit is then opened and the CO_2 is fluxed through the permeable electrode. The IL at the interface with the permeable electrode starts reacting with CO_2, leading to the IL + CO_2 formation. The capture of the CO_2 alters the charge distribution in the anion modifying the interface potential drop from $\Delta V_{IL/el}$ to $\Delta V_{IL+CO_2/el}$ only at the permeable electrode (see Figure 4b). The drive for the potential change is the minimization of the free energy at the interface that forces the anions to alter their orientation. Besides accumulating close to the interface, IL + CO_2 also slowly diffuses toward the counter electrode forming a smooth interface between the pure IL and the one the captured CO_2. Two distinct areas form on the two sides of the device, one mainly constituted by IL + CO_2 (close to the permeable electrode) and one by pure IL (close to the counter electrode), separated by a mixed phase in between. The two areas have different bulk potential level, so a potential drop, $\Delta V_{IL+CO_2/el}$ arises in the electrolyte.

The measured open circuit voltage variation, after CO_2 is fluxed in, is then the result of two effects: the ion reorientation and the difference in bulk potential. As noticeable in Figure 4b, the change in anion orientation at the permeable electrode lowers the overall potential of the left electrode, whereas the difference in bulk level, instead, increases the left electrode potential. The sign of the measured open circuit voltage is determined by the effect that dominates with the specific IL used as electrolyte.

In the analysis of the potential drops, we assumed, for simplicity, the total conversion of [Im] in [$ImCO_2$] during the CO_2 fluxing. The real amount is dictated by the stationary nonequilibrium state given by the pressure of CO_2 and the surface mobility of anions and the diffusion coefficient of [$ImCO_2$] toward the bulk. Nevertheless, such approximation does not alter the provided qualitative picture. Both the size of the potential drop at the

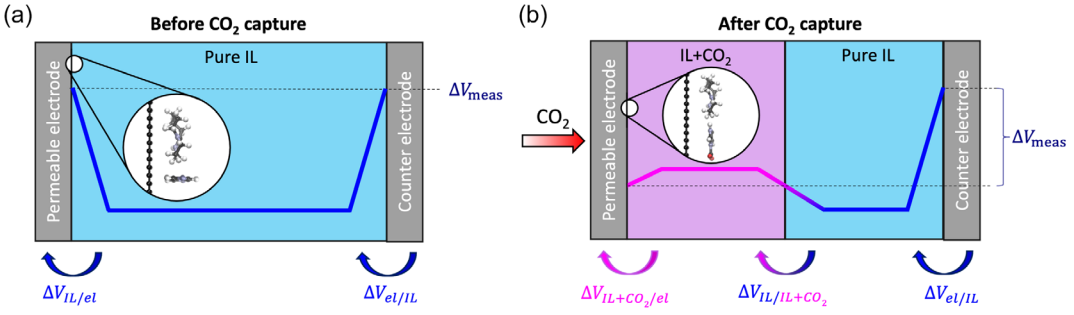

Figure 4. a) Sketch of the device before and b) after CO_2 capture showing the origin of the voltage variation measured experimentally. The insets show the qualitative molecular orientation of the IL at the interface with the electrode in the two cases.

interface with the electrode and the difference in bulk levels between [DBUH][Im] and [DBUH][$ImCO_2$] are directly proportional to the number of [$ImCO_2$] in the IL. The two quantities vary consistently so the working mechanism is the same independently from the number of converted anions. A lower number is likely to lead to a smaller measured voltage.

4. IL Dilution

To improve the energetic yield of the entire system, it was proposed to act on the electrolyte by diluting it. This step is expected to improve the electrochemical performances of the device, in terms of coulombic efficiency, energetic efficiency, self-discharge, and equivalent series resistance (ESR). It was decided to test two kinds of dilution following two different strategies. In the first case, the idea was to exploit an IL showing the best performances from a supercapacitive point of view: the choice fell on the [Emim][Ac] because of good compatibility with [DBUH][Im], CO_2 absorption capabilities, and higher conductivity at pure state. Compared them with **Figure 5**a, what stands out is that [Emim][Ac] has a conductivity about 5 times higher than [DBUH][Im], namely, 0.56 mS cm^{-1} for [DBUH][Im] and 2.45 mS cm^{-1} for [Emim][Ac].

The second type of dilution has the goal of increasing the ionic mobility (and so the conductivity) by acting on the viscosity of the electrolyte and on the reduction of ion–ion interactions through the solvation of charged species to reduce the self-discharge. This is done by using polar aprotic solvents with high dielectric constant and low viscosity[24] such as PC. With the aim of choosing the best dilution configuration for each of those proposed solutions, some conductivity tests were taken on.

Figure 5a shows a very different behavior of the chosen solutions, which however was expected since in the first case ([DBUH][Im] in [Emim][Ac]), both the solute and the solvent are conductive electrolytes, while PC acts as a dielectric. In fact, in this second case, a too-high dilution leads to low conductivity because of the poor ionic concentration, while with too light dilution, the conductivity decreases because the ion pairing hinders the overall ion mobility. In the case of the mix of two ILs, the issue due to conductivity decrease at low concentrations is not observable, since in this region conducting properties are controlled by the most present IL.

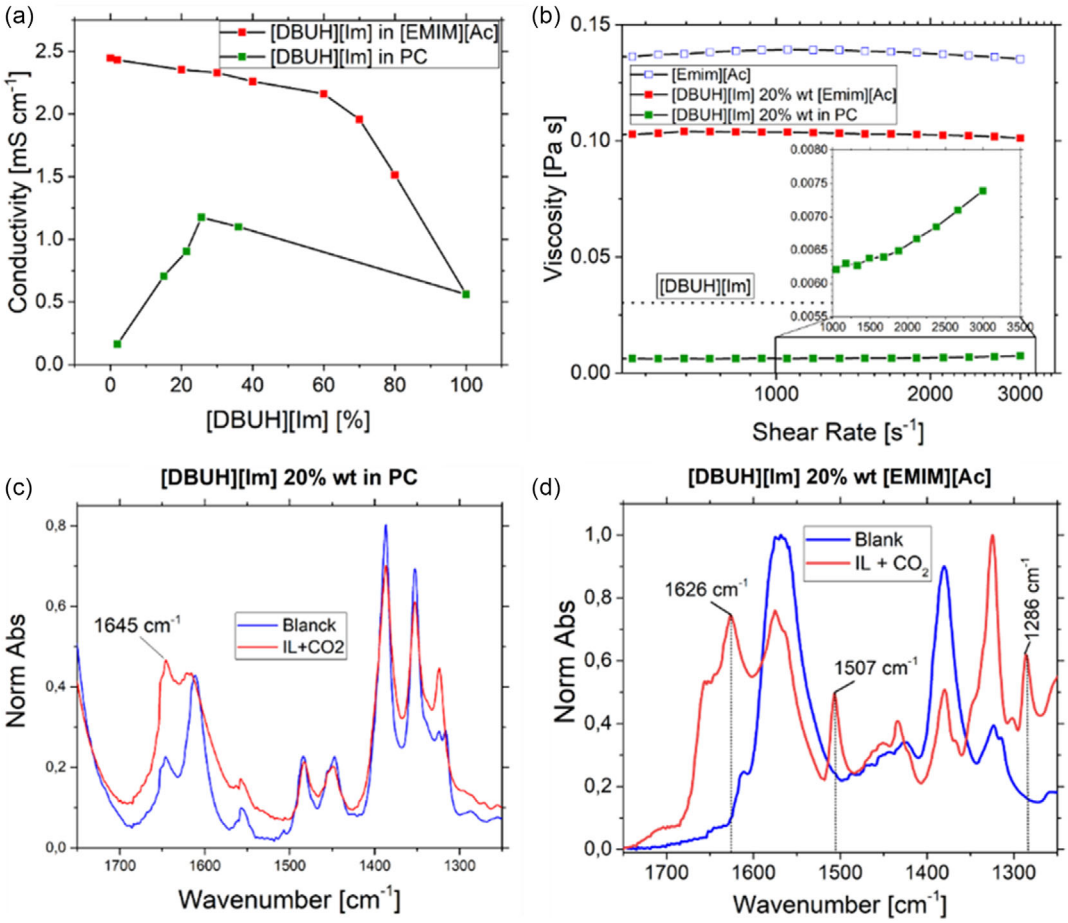

Figure 5. a) Conductivity measurements at different concentrations of [DBUH][Im] in PC (green dots) and in [Emim][Ac] (red dots), b) the comparison of viscosity among [DBUH][Im] and [Emim][Ac] and the two selected dilutions, c) infrared spectra of [DBUH][Im] solution in PC 1M before (black), after the absorption of CO_2 (red), and after degassing (Blue), and d) infrared spectra of [DBUH][Im] [Emim][OAc] 20:80 before (black), after the absorption of CO_2(red), and after degassing (blue).

For both solutions, it was selected a dilution close to 20% wt of [DBUH][Im]: this decision came from the fact that for the [Emim][Ac]-based solution, this concentration ensures a conductivity very close to the maximum possible and at the same time ensures a presence of [DBUH][Im] sufficient to participate in an active way to the harvesting of the energy coming from CO_2 capture. For PC-based solution, the maximum conductivity value was detected as around 20% wt of concentration.

Viscosity measurements were again performed (reported in Figure 5b) using a continuous mode analysis applying an increasing shear rate from 500 to 3000 s^{-1}. As previously explained, the mixture of [Emim][Ac] and [DBUH][Im] produced a drastic increase in the viscosity, which however does not worsen the electrochemical performances of the device, as explained in the following sections (an increase in viscosity of more than 3 times was detected, from 30.3 mPa s^{-1} of undiluted IL, to 103.7 mPa s^{-1} of [Emim][Ac] diluted mixture). This behavior was expected since the diluent has a much higher viscosity compared to [DBUH][Im]. In contrast, while exploiting PC, the viscosity has a strong decrease, reaching a viscosity 10 times smaller than starting value. Moreover, a non-Newtonian behavior of this solution is noticeable. In particular, it has a shear-thickening acting.

A solution of [DBUH][Im] in PC 1 M was tested for CO_2 adsorption, to understand the role of PC as solvent the adsorption of polycarbonate alone was also tested. The solubility of CO_2 into PC is in line with what expected from literature[25] with a molar fraction more or less around 0.01 at 1 atm and 25 °C (Table S1, supporting information) as expected from a physical sorption. The addition of [DBUH][Im] highly improves the solubility of CO_2 in the solution. The ratio of adsorption in function of [DBUH][Im] in this case is 0.9 mol of CO_2 each mol of [DBUH][Im]. The infrared analysis of the two adsorptions confirms the gravimetric analysis. In the case of PC, there is no change in the infrared spectra as the assessment of physical adsorption of CO_2 is disturbed by the atmospheric CO_2 compensation of the instrument (spectrum reported in supporting information). In the case of [DBUH][Im], Figure 5c, the formation of carbamate is confirmed by the appearance of the same peaks of pure [DBUH][Im] around 170–1600 cm^{-1}.

In contrast, the mixing between [DBUH][Im] and [Emim][OAc] with a 1:4 ratio shows an increase in adsorption similar to pure [Emim][OAc], however, the main feature of this mixing is the lack of gelification after CO_2 sorption. The adsorption behavior is similar to pure [Emim][OAc] with a negligible increase of CO_2 adsorbed, however, the infrared analysis (Figure 5d) shows that in this case there are two different species because in the range 1700–1500, there are two different carbamate stretching, one at about 1665 cm^{-1} and the other at about 1645 cm^{-1} probably the two different imidazolium and the imidazolate are both partially adsorbing the CO_2 with formation of similar species.

5. Optimized CO_2CAP Process

Exploiting the so-defined new compositions of electrolyte, two more devices were built in symmetric configuration with GDL electrodes (d = 18 mm) and a separator wetted with 150 µl of electrolyte. Impedance spectroscopy and cyclic voltammetry (reported in supporting information) were performed to check how the dilution affects the cell characteristics.

Comparing the data reported in **Figure 6**a,b, it is clear how both the proposed dilutions show an improvement in EC performance. In particular, the change in the electrolyte does not produce great differences in capacitance value, which remains stable around 0.3 mF cm^{-2}, but it is possible to observe an increase of 10% in energy efficiency and an improvement for the coulombic efficiency (from 90% to 95%).

Applying the same kind of CapMix procedure described above, it was found possible to obtain a linearization of the V versus Q plot. Moreover, thanks to the dilution, it was possible to harvest more energy than the one needed to charge the device prior to CO_2 absorption.

In Figure 6c–e, the comparison between the three proposed devices shows how diluting the electrolyte allows harvesting energy from the CapMix cycle since it is possible to obtain a closed curve traveled in a counterclockwise direction. In particular, it is possible to notice how the recovered energy is approximately the same for all three devices. What allows us to obtain a positive net energy balance is the reduction of the charging energy. Considering discharge power, Figure 6f confirms the improvement of the device: diluting the electrolyte, it is possible to achieve higher power densities.

From Figure 6d, it can be found that the slope of the charging and the discharging step is the same, this means that there is no capacitance change during the cycle, so it is not possible to talk about CapMix in its classical meaning, confirming predictions of simulations performed. According to Brogioli et al.[20] capacitive mixing process based on capacitive double-layer expansion is possible only if the double layer of ions at electrode–electrolyte interface changes its thickness and in this way produces a change in the overall capacitance. Since this capacitance change was not detected, it is reasonable to imagine that the mechanism behind this phenomenon is a different one. This hypothesis was proven by performing some absorption/desorption cycles around OCP (shown in **Figure 7**a). It was possible to observe a change in voltage also without the induction of an EDL.

The operation with N_2 can be easily explained within our proposed mechanism. After the absorption of CO_2, there is an unbalance in the potential between the two electrodes due to the asymmetry of the two electrode/IL interfaces (see Figure 3e). The following constant current discharge (CCD) moves electrons from one electrode to the other to counteract such an unbalance so that the measured V is zero again. Once N_2 is fluxed the two interfaces return to be characterized by the same IL, [DBUH][Im]. However, the charge on the two contacts is no longer equal so a nonzero ΔV_{meas} is measured. The absolute excess charge needed to zero out the device voltage after the CO_2 absorption stage is conserved during the regenerative N_2 stage, resulting in a negative device voltage as the system is fully restored. A supplemental CCD stage is required to remove the excess of charge and recover the initial state of Figure 3d.

It was proposed to avoid the floating step and try to operate the device around 0 V. This decision came from the observation that also in uncharged conditions (OCV) a stream of gas can produce a potential difference between the electrodes (Figure 7a). The procedure for energy harvesting was modified as follows

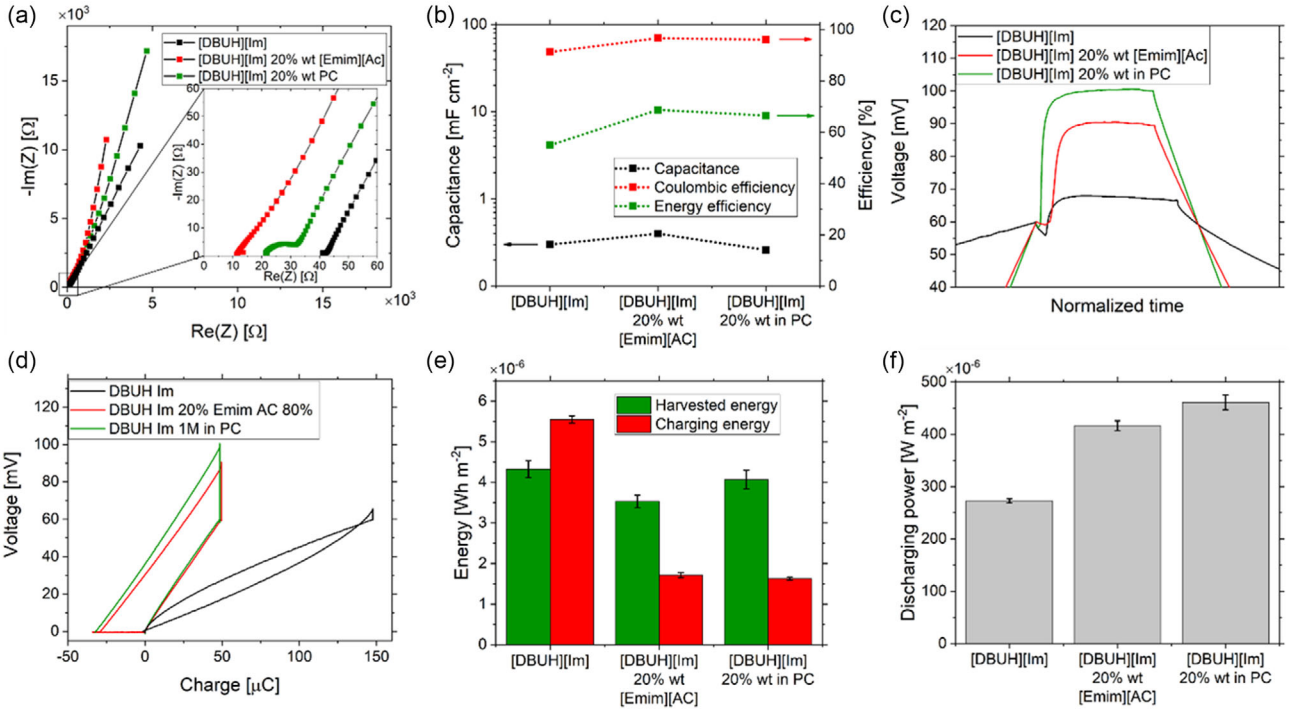

Figure 6. a) Nyquist plot of the three different proposed devices, b) sum up of the figure of merit evaluated from cyclic voltammetry measurements (reported in supporting information, c,d) the actual measurement of the CapMix cycles performed with the three proposed devices, and e,f) energy and power extracted from the CapMix cycles.

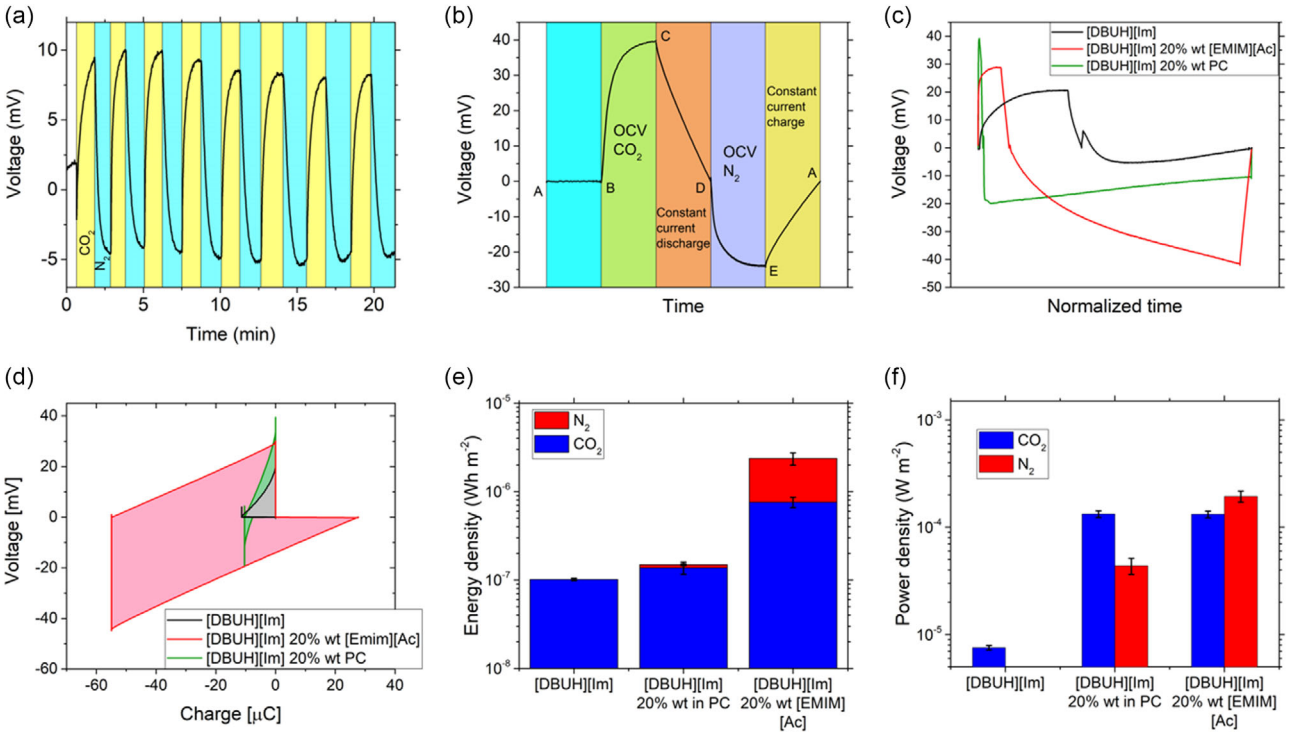

Figure 7. a) Cycles of absorption/desorption of CO_2 around OCV, used to detect a change in cell voltage even in absence of any external polarization, b) schematic procedure of the updated CapMix cycle around 0 V, c,d) the actual measurement of the CapMix cycles performed with the three proposed devices, and e,f) energy and power extracted from the CapMix cycles.

(Figure 7b): 1) short circuit hold for 5' to allow the system to recover at each repetition the same starting conditions; 2) setting open circuit conditions and flush CO_2 (50 mL min^{-1}) inside the device. This causes a positive change in OCV. The gas stream is held until it reaches a peak in voltage. When this condition is verified, gas flush is stopped, and it is possible to proceed to the next step; 3) the voltage change can be discharged on an external load (so to recover the energy related to the capture of CO_2). This step is performed applying a constant current equal to 1 μA cm^{-2} until reaching 0 V; 4) after the complete discharge of the device, open circuit conditions are set back and a stream of nitrogen (50 mL min^{-1}) is imposed. N_2 in this step is adopted to remove the CO_2 absorbed in step 2 (in this stage, the electrolyte is regenerated). The gas flow is held for a fixed time, chosen with the aim of ensuring the repeatability of the process; and 5) after the regeneration in N_2, OCV has fallen to a negative value. It is possible to recover energy also in this phase, so also a negative change of voltage produces a positive harvesting of energy.

In Figure 7c,d, comparison among the three devices proposed until now is reported. At first glance, it becomes evident how dilutions produced an improvement in terms of voltage rise: 10 mV higher in case of [EMIM][Ac] dilution and the double in case of PC dilution. Other visible effects are the reduction of the absorption time interval and the positive energy balance. In particular, the shortest absorption time is obtained for PC dilution (from 300" of [DBUH][Im] in undiluted conditions to 5"), while the dilution in [EMIM][Ac] produces a harvested energy 10 times greater than the first device proposed.

Since it is well known that [EMIM][Ac] interacts with CO_2 capturing it, some tests were performed on a device based on unmixed [EMIM][Ac], to evaluate its contribution to the CapMix cycle. These tests proved a negligible contribution to the harvested energy. Data and details are reported in supporting information.

Previous analyses support the mechanism proposed in this article and further show the departure from CapMix. For the device to work, it is not necessary for the contacts to be initialized to a given floating voltage like in CapMix case because the phenomenon is not based on EDL expansion.

6. Electrode Optimization

Once changed the composition of electrolyte and improved the conductivity of the entire device and enhanced the efficiencies, the remaining parameter to work on is the capacitance. This can be increased by acting on the electrodes. The strategy adopted is to deposit a slurry of activated carbons (AC) over the GDL by doctor blade method, immediately followed by a drying step at 60 °C overnight. The electrode is then calendered to increase the contact points between the active material and the current collector, thus reducing the ESR and improving both efficiencies and capacitance.[26,27]

The electron microscopy was employed to study the morphology of the GDL electrodes, both as they are (Figure S16a, Supporting Information) and coated with AC (Figure S16b, Supporting Information). In the top view, it is possible to appreciate the porosity of the GDL and the uniformity of the AC layer on top of it. In the cross-section (Figure S16c,d, Supporting Information), it shows the effect of the calendering process, which caused the compression of the GDL down to 200 μm. The compression affected both the GDL and the AC coating on top of it, reducing their thicknesses of ≈30%. The GDL thickness decreased from 230 μm down to 180 μm, while the AC thickness from 30 μm down to 20 μm.

The electrodes described in the previous section were then tested in both dilutions proposed. In this new configuration, it is necessary to also consider the resistive contribution due to the presence of activated carbons on the surface of GDL and the much higher porosity introduced. Because of this, in this case, it is necessary to find the proper way to make electrodes compatible with the electrolytes. PC-based electrolyte is characterized by a much lower viscosity, if compared to [DBUH][Im] electrolyte. The overall effect is a reduction of the real part of the impedance and it allows a better wettability of the electrode's surface, making it possible to use this dilution also at room temperature.

In contrast, the same reasoning cannot be applied to the [EMIM][Ac]-based dilution. In this case, the viscosity is much higher (100 mPa s vs 6.5 mPa s), causing a poor wettability of activated carbons. To manage this issue, it was decided to let this device work at 60 °C; in this way, it is possible to reduce electrolyte viscosity and improve device electrochemical performances.[28]

The influence of AC-based electrodes was tested by performing cyclic voltammetry and impedance spectroscopy as done in all previous measurements. Results are reported in **Figure 8**a,b. ESR and capacitance are greatly improved, while coulombic efficiency remains stable. Focusing on the energy efficiency, what comes out is that the action of the temperature increases it, while only adding AC over GDL produces a dramatic decrease.

Going on with the testing, the characterized devices were then used to harvest energy. If the PC-based electrolyte has no particularity in terms of capturing procedure since it is similar to the one already described, some considerations are required for the [DBUH][Im] 20% wt [Emim][Ac] 80% wt device, which works at 60 °C. In fact, both ILs mixed are designed for CO_2 capture, and in literature it has been shown that temperature can affect the capture ability. Temperature has an effect both on the CO_2 solubility in the IL medium and on the viscosity of the IL: higher temperature leads to a decrease in the solubility of CO_2, in contrast, the increase of temperature leads to a reduction of IL viscosity, promoting the mass transport. Combining these two influences, it is possible to conclude that the optimal temperature for CO_2 capture is placed between 50 and 60 °C.[29]

Testing these configurations, it is possible to achieve the highest values of energy gain and extracted power (Figure 8e,f). For these CapMix procedures, the parameters used are the same as all previous experiments except for the current applied which was requested to be increased up to 10 μA cm^{-2} for [DBUH][Im] 20% in [Emim][Ac] and to 4 μA cm^{-2} for [DBUH][Im] 20% wt in PC, because of the much higher capacitances compared to all previous cases. In particular, for the device characterized by the dilution with [Emim][Ac] heated at 60 °C, it was possible to achieve a harvested energy equal to 40 μWh m^{-2}, which is 400 times greater than the energy recovered with the first device proposed

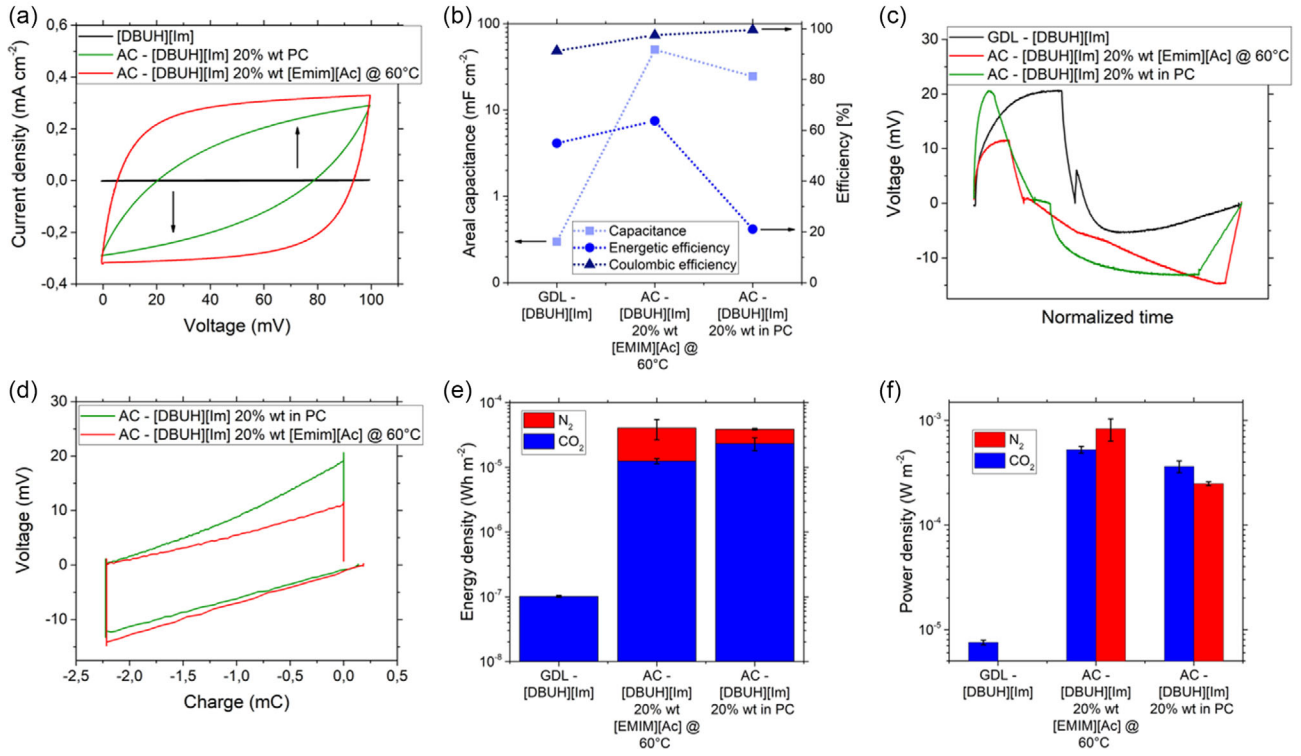

Figure 8. a) Activated carbon effect on the cyclic voltammetry of the devices with all the electrolyte analyzed, b) figures of merit extracted from CV measurements, c,d) the actual measurement of the CapMix cycles performed with the new proposed devices, and e,f) energy and power extracted from the CapMix cycles.

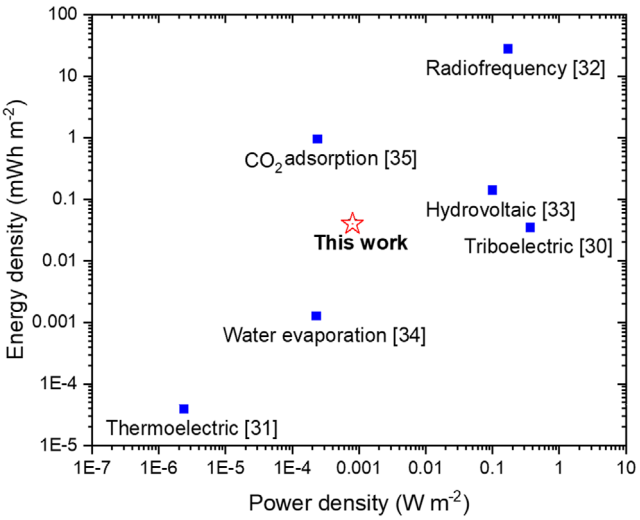

Figure 9. Ragone plot of the presented work and previous papers about emerging energy storage systems from nonconventional sources.

(undiluted [DBUH][Im]). To have a direct comparison between the proposed device and other technologies reported in literature, it was decided to report a Ragone plot. As shown in **Figure 9**, CO2CAP preliminary results match the performances of other emerging energy storage systems from nonconventional sources.[30–35]

7. Conclusion

We demonstrated for the first time the energy harvesting from CO_2 absorption/desorption into an electrochemical capacitor based on IL as electrolyte and CO_2 absorption medium. The experimental and modeling results clearly show that the working principle of this system cannot be further ascribed to EDL expansion as in traditional capacitive mixing devices based on water electrolytes. Our studies identify that the energy harvesting in the present device is the result of two competing effects, ion reorientation at the interface induced by the CO_2 absorption and difference in bulk potentials between the pristine IL and the one that captured CO_2, that induce a potential variation during the CO_2 capture process. This reflects on the OCP of the electrodes and finally on the OCV of the cell with a positive net energy gain in the absorption/desorption CO_2 cycle that is synchronized with the charge and discharge of the electrochemical capacitor.

When verified the new mechanism, several optimizations were implemented. Dilutions of the IL notably improved voltage rise while this harvesting mechanism allows to work around the OCP without the need of an external power supply. Indeed, the CO2CAP device works by exploiting the chemical reaction between IL and carbon dioxide that occurs just in one half of the cell and does not directly rely on the electrode's charge. Moreover, in this way, it is possible to harvest energy both from CO_2 absorption and when flushing N_2 to desorb CO_2. Finally,

increasing the capacitance of the electrodes, it is possible to further improve the CO2CAP performances achieving the power density of 0.8 mW m^{-2}.

8. Experimental Section

Materials Characterization: Electron microscopy characterization was carried out with a field-emission scanning electron microscope (FESEM Supra 40, manufactured by Zeiss) equipped with a Si(Li) detector (Oxford Instruments) for energy-dispersive X-ray spectroscopy.

Rheology measurements were performed in a parallel disk rheometer MCR 302, manufactured by Anton Paar, exploiting a 25 mm diameter parallel disk configuration, with a distance between the plates equal to 0.6 mm. The temperature was controlled through the internal Peltier system and before each temperature point, the system was let thermalize for 10 min.

Attenuated total reflection infrared spectroscopy (ATR-IR) was employed to characterize the membranes. Measurements were carried out on a Bruker Tensor II Fourier transform spectrophotometer. The spectra were acquired by accumulating 64 scans (64 for the background spectrum) in 4000–600 cm^{-1} range with a resolution of 2 cm^{-1}.

The CO_2 absorption capacity of ILs and solutions was determined using gravimetric absorption. The sample was insufflated with CO_2 and the weight increase was recorded as a function of time until constant weight. A small portion of the solutions was sampled, stored in vials saturated with CO_2, and subjected to ATR-IR. The remaining part was subjected to nitrogen insufflation and the weight loss was recorded until constant weight.

Gravimetric measurements. The CO_2 loading of ILs and solution was quantified using a gravimetric method as reported previously.[36] ≈3 mL of solution was poured in a batch reactor (≈4.5 mL), purged for 10 min with N_2 (30 mL min^{-1}), and weighted. Then, CO_2 (30 mL min^{-1}) was bubbled until no mass increase was observed. The captured CO_2 was calculated by mass difference before and after CO_2 contact, considering the reactor headspace contribution. CO_2 over the total mass was evaluated. Desorption was performed by purging for with N_2 (30 mL min^{-1}) and weighting the sample. The operation was continued until constant weight was achieved. For this characterization, see Supporting Information.

The electrochemical measurements were performed with a VMP3 potentiostat manufactured by Bio-Logic. Galvanostatic measurements were performed with Arbin BT2000.

Electrochemical Cell Design: To perform the materials characterization, it is necessary to use two and three electrodes measurements, respectively, 2 E and 3 E; to do that, two different types of cells were used.

The most important characteristics for the 2 E measuring cell are the isolation of the capture media from the external environment and the possibility of flowing gas through the cell. For these reasons, we selected the ECC-air test cell provided by EL-CELL GmbH company (Figure S5, Supporting Information).

The core of the cell is positioned into the cell base, and it is composed of two gas diffusion layers (d = 18 mm) and a polymeric separator (d = 18 mm) that avoids any undesired short-circuit between the two electrodes; 150 µL of electrolyte was dispensed on the top of the separator (Figure 1a).

The current collector placed on the upper GDL also includes a perforated plate that ensures both electrical connection and gas flow. The two ports placed in the cell lid allow the flush of the gas inside the cell and drain it out.

Two EL-FLOW Select provided by Bronkhorst flow technology were used to control the flows of N_2 and CO_2 gases. The pneumatic connections (pipes, valves, and connectors) between the test cell, flow meters, and gas cylinders were constituted by Swagelok components.

Experimental Protocol Design and Electrochemical Characterization: Operative voltage measurements (OVMs) were performed to let the device work in electrochemical stable conditions. OVM consists of repeated anodic and cathodic voltammetric scans at relatively low scan rates of 5 mV s^{-1} of increasing polarization levels. This procedure allows the retrieval of information to balance the electrode charges to exploit the maximum cell voltage. Electrochemical impedance spectroscopy measurements were used as figures of merits to ensure charge-balancing calculations relying on similar experiments.

Assembled devices were subject to electrochemical conditioning by applying a constant voltage to remove any possible side effects that could minimize the phenomenon to be observed. In this way, all the devices under test were assumed to be comparable.

A two-stage electrochemical test procedure for verifying the CO_2 CapMix procedure harvesting process was performed. In the first stage, the device is charged at a constant current until a specific voltage is reached. The voltage and retention time are varied to investigate their influence on the harvesting process. The extended retention time at constant voltage helps reduce leakages at the porous electrode. After this period, CO_2 is flushed out, and the device is discharged at a constant current as the voltage rise reaches its maximum value.

Modeling: Classical molecular dynamics simulations were used to provide insights into the working mechanism of the device. The calculations were performed in LAMMPS.[37] The device was simulated as two 30 Å × 30 Å parallel planes of graphene sandwiching the IL under investigation. The positions of the graphene ions were fixed during the simulation. Graphene was taken as representative of the carbon-based electrodes used in the experimental device, as in several previous simulations.[38,39] Three ILs were studied: [DBUH][Im], [DBUH][ImCO_2], and a mixture containing 50% of the former IL and 50% of the latter. Each IL was constituted by 300 ion pairs. The distance between the electrodes is not fixed but it varies accordingly to the IL density, so to find it ambient pressure was applied to one of the graphene sheets so that it could rigidly move toward the other.[40,41] The system is equilibrated at 600 K for 10 ns with the movable graphene sheet. The use of high temperature is a common method to accelerate phenomena like diffusion or reactions in molecular dynamics.[42–45] Afterward, the temperature is lowered to 400 K. The system is given 5 ns to readjust to the new temperature. In the following 5 ns the position of the pressured graphene is monitored to find the equilibrium value. The sheet is then blocked in the average position and the IL is equilibrated again for 2 ns. 40 ns of production run at the same temperature follow for the extraction of equilibrium quantities. In all cases, the system was thermostated with the Nosé–Hoover thermostat and the time was integrated every 1 fs. Periodic boundary conditions were applied in all directions. To avoid replica interactions, at least 100 Å of vacuum was put in between. For the identification of the IL bulk level, the simulation box was enlarged to accommodate two IL, [DBUH][Im] and [DBUH][ImCO_2], of 150 ion pairs each. The ILs were separated by a vacuum layer of 130 Å. Each IL was kept in position by two harmonic walls (flat walls that interact with IL atoms by a repulsive only potential) replacing the graphene sheets. The distance at which the walls were placed reproduced the density of the ILs found in the previous calculations.

For all the simulations, to obtain the electric potential across the interface, the charge distribution was first calculated by assigning to each atom a small Gaussian with height proportional to the atom charge. The trajectory was sampled every 0.05 ns and the final charge distribution was the result of an average of all the instantaneous distributions. To improve the statistics the data from symmetrical interfaces were averaged together. Poisson's equation was then used to derive the electric potential.

To describe atomic interactions in the IL, the general AMBER force field (GAFF2),[46] known for accurately reproducing ILs,[47] was employed. The charges on each atom were obtained by Hartree–Fock simulations with a 6–31 G(d) basis set using GAMESS software.[48] The aim of the Hartree–Fock simulations was to calculate the electrostatic potential of the molecules composing the ILs. RESP algorithm then found the point charges that best reproduced such potential.[49] Charges were then scaled by 0.8 to avoid the typical artificial overstructuring occurring to the ILs.[50,51] Hartree–Fock simulations were also employed to validate the GAFF2 potential. Almost all coefficients gave satisfactory results. However, for [ImCO_2], the bond between the imidazole nitrogen and the CO_2 was not well described by the harmonic potential typically used in GAFF2. The bond potential was changed in Morse and the reparameterization was carried out with Hartree–Fock. The carbon atoms of the

graphene electrodes were simply described by a 12–6 Lennard–Jones with paraments taken from GAFF2.

Materials: All the electrodes used in this work were based on Sigracet gas diffusion layer (GDL) 28 BC from SGL carbon. To increase the overall capacitance, in some configurations, it was decided to add on top of these GDL a carbon slurry produced by mixing together in a water-based solution an amount of 85% wt activated carbons (YP–50 F from Kuraray), 10% wt carbon black (Timical Super C65 from Imerys), and 5% wt sodium carboxymethyl cellulose (from MTI, average M_w 400 000). GDL electrodes were cut before assembling the cell in an 18 mm diameter circular shape and dried at 120 °C for 12 h in low vacuum condition inside a glass oven B-585 from Büchi. The polymeric separator was supplied by El-Cell, namely, FS-5 P (Freudenberg Viledon FS 2226 E + Lydall Solupor 5P09B). All the electrochemical cells were assembled in an Mbrown glove box filled with nitrogen. The oxygen and moisture levels were below 0.5 ppm.

1,8-Diazabicyclo-undec-7-ene (98%), imidazole (99%), methanol (98%), and PC 99.7% from Sigma-Aldrich and 1-Ethyl-3-methylimidazolium acetate ([EMIM][Ac]) 95% from Iolitec were used and evaluated as diluting solvents.

1,8-Diazabicyclo[5.4.0]undecanium Imidazolide ([DBUH][Im]) was prepared by slightly modifying a previously reported reaction.[15] A 50%wt 1,8-Diazabicyclo-undec-7-ene solution in methanol was neutralized by using a equimolar quantity of imidazole (Figure S1, Supporting Information). After reaction, methanol was evaporated by using a rotavapor, and the IL was dried at 60 °C for 24 h before use in the vacuum drying in which the vacuum degree is lower than 133 Pa.

Supporting Information

Supporting Information is available from the Wiley Online Library or from the author.

Acknowledgements

This work is part of the project CO2CAP that has received funding from the European Research Council (ERC) under the European Union's ERC starting grant agreement no. 949916.

Conflict of Interest

The authors declare no conflict of interest.

Author Contributions

Davide Molino: methodology (lead); writing—original draft (equal). **Federico Raffone**: methodology (equal); software (lead); writing—original draft (equal). **Pietro Zaccagnini**: conceptualization (lead); methodology (equal); writing—original draft (equal). **Alessandro Pedico**: investigation (equal); methodology (equal); writing—original draft (equal). **Simone Martellone**: methodology (equal); writing—original draft (supporting). **Giuseppe Ferraro**: investigation (equal); writing—original draft (equal). **Sergio Bocchini**: conceptualization (equal); methodology (equal); writing—original draft (equal). **Giancarlo Cicero**: investigation (equal); writing—original draft (equal). **Andrea Lamberti**: funding acquisition (lead); investigation (equal); methodology (equal); supervision (lead); validation (equal); writing—original draft (equal). **Davide Molino** and **Federico Raffone** contribute equally to this work.

Data Availability Statement

The data that support the findings of this study are available from the corresponding author upon reasonable request.

Keywords

capacitive mixing, CO_2 emissions, electrochemical capacitors, energy harvesting, ionic liquids

Received: January 14, 2025
Revised: March 18, 2025
Published online: April 6, 2025

[1] F. A. Rahman, M. M. A. Aziz, R. Saidur, W. A. W. A. Bakar, M. R. Hainin, R. Putrajaya, N. A. Hassan, *Renewable Sustainable Energy Rev.* **2017**, *71*, 112.
[2] D. Stolten, *Chem. Eng. Technol.* **2012**, *35*, 407.
[3] H. Lepaumier, D. Picq, P.-L. Carrette, *Ind. Eng. Chem. Res.* **2009**, *48*, 9061.
[4] J. D. Holbrey, K. R. Seddon, *Clean Technol. Environ. Policy* **1999**, *1*, 223.
[5] M. E. Boot-Handford, J. C. Abanades, E. J. Anthony, M. J. Blunt, S. Brandani, N. Mac Dowell, J. R. Fernández, M.-C. Ferrari, R. Gross, J. P. Hallett, R. S. Haszeldine, P. Heptonstall, A. Lyngfelt, Z. Makuch, E. Mangano, R. T. J. Porter, M. Pourkashanian, G. T. Rochelle, N. Shah, J. G. Yao, P. S. Fennell, *Energy Environ. Sci.* **2014**, *7*, 130.
[6] H. Zhou, X. Wang, E. Sheridan, H. Gao, J. Du, J. Yang, D. Chen, *J. Electrochem. Soc.* **2016**, *163*, A2618.
[7] C. Merlet, B. Rotenberg, P. A. Madden, P.-L. Taberna, P. Simon, Y. Gogotsi, M. Salanne, *Nat. Mater.* **2012**, *11*, 306.
[8] P. Simon, Y. Gogotsi, B. Dunn, *Science* **2014**, *343*, 1210.
[9] G. Wang, L. Zhang, J. Zhang, *Chem. Soc. Rev.* **2012**, *41*, 797.
[10] J. Chmiola, C. Largeot, P.-L. Taberna, P. Simon, Y. Gogotsi, *Angew. Chem. Int. Ed.* **2008**, *47*, 3392.
[11] J. B. Goodenough, *Energy Environ. Sci.* **2014**, *7*, 14.
[12] D. Brogioli, *Phys. Rev. Lett.* **2009**, *103*, 058501.
[13] H. V. M. Hamelers, O. Schaetzle, J. M. Paz-García, P. M. Biesheuvel, C. J. N. Buisman, *Environ. Sci. Technol. Lett.* **2014**, *1*, 31.
[14] T. Kim, B. E. Logan, C. A. Gorski, *Environ. Sci. Technol. Lett.* **2017**, *4*, 49.
[15] X. Zhu, M. Song, Y. Xu, *ACS Sustain. Chem. Eng.* **2017**, *5*, 8192.
[16] D. Skarpalezos, A. Tzani, E. Avraam, C. Politidis, A. Kyritsis, A. Detsi, *J. Mol. Liq.* **2021**, *344*, 117754.
[17] W. Xiong, M. Shi, L. Peng, X. Zhang, X. Hu, Y. Wu, *Separation Purif. Technol.* **2021**, *263*, 118417.
[18] M. Izadyar, M. Rezaeian, A. Victorov, *Phys. Chem. Chem. Phys.* **2020**, *22*, 20050.
[19] D. J. G. Ives, G. J. Janz, C. V. King, *J. Electrochem. Soc.* **1961**, *108*, 246C.
[20] D. Brogioli, R. Ziano, R. A. Rica, D. Salerno, O. Kozynchenko, H. V. M. Hamelers, F. Mantegazza, *Energy Environ. Sci.* **2012**, *5*, 9870.
[21] A. Lasia, *J. Phys. Chem. Lett.* **2022**, *13*, 580.
[22] O. Gharbi, M. T. T. Tran, B. Tribollet, M. Turmine, V. Vivier, *Electrochim. Acta* **2020**, *343*, 136109.
[23] F. Raffone, A. Lamberti, G. Cicero, *Electrochim. Acta* **2023**, *458*, 142344.
[24] V. Ruiz, T. Huynh, S. R. Sivakkumar, A. G. Pandolfo, *RSC Adv.* **2012**, *2*, 5591.
[25] Z. Zhao, Y. Huang, Z. Zhang, W. Fei, M. Luo, Y. Zhao, *J. Chem. Thermodyn.* **2020**, *142*, 106017.
[26] S. Dsoke, X. Tian, C. Täubert, S. Schlüter, M. Wohlfahrt-Mehrens, *J. Power Sources* **2013**, *238*, 422.
[27] G. A. Safitri, K. Nueangnoraj, P. Sreearunothai, J. Manyam, *Curr. Appl. Sci. Technol.* **2020**, *20*, 124.
[28] B. E. Conway, *Electrochemical Supercapacitors: Scientific Fundamentals and Technological Applications*, Springer, Berlin, New York **2013**.
[29] M. Alvarez-Guerra, J. Albo, E. Alvarez-Guerra, A. Irabien, *Energy Environ. Sci.* **2015**, *8*, 2574.

[30] S. Li, Y. Fan, H. Chen, J. Nie, Y. Liang, X. Tao, J. Zhang, X. Chen, E. Fu, Z. L. Wang, *Energy Environ. Sci.* **2020**, *13*, 896.
[31] Z. A. Akbar, J.-W. Jeon, S.-Y. Jang, *Energy Environ. Sci.* **2020**, *13*, 2915.
[32] F. Meder, A. Mondini, F. Visentin, G. Zini, M. Crepaldi, B. Mazzolai, *Energy Environ. Sci.* **2022**, *15*, 2545.
[33] C. Liu, S. Wang, X. Wang, J. Mao, Y. Chen, N. X. Fang, S.-P. Feng, *Energy Environ. Sci.* **2022**, *15*, 2489.
[34] W. Deng, G. Feng, L. Li, X. Wang, H. Lu, X. Li, J. Li, W. Guo, J. Yin, *Energy Environ. Sci.* **2023**, *16*, 4442.
[35] Z. Wang, T. Hu, M. Tebyetekerwa, X. Zeng, F. Du, Y. Kang, X. Li, H. Zhang, H. Wang, X. Zhang, *Nat. Commun.* **2024**, *15*, 2672.
[36] G. Latini, M. Signorile, F. Rosso, A. Fin, M. d'Amora, S. Giordani, F. Pirri, V. Crocellà, S. Bordiga, S. Bocchini, *J. CO2 Util.* **2022**, *55*, 101815.
[37] A. P. Thompson, H. M. Aktulga, R. Berger, D. S. Bolintineanu, W. Michael Brown, P. S. Crozier, P. J. in 't Veld, A. Kohlmeyer, S. G. Moore, T. D. Nguyen, R. Shan, M. J. Stevens, J. Tranchida, C. Trott, S. J. Plimpton, *Comput. Phys. Commun.* **2022**, *271*, 108171.
[38] Y.-J. Tu, J. G. McDaniel, *J. Phys. Chem. C* **2021**, *125*, 20204.
[39] S. A. Kislenko, I. S. Samoylov, R. H. Amirov, *Phys. Chem. Chem. Phys.* **2009**, *11*, 5584.
[40] G. Tronci, F. Raffone, G. Cicero, *Appl. Sci.* **2018**, *8*, 1547.
[41] F. Risplendi, F. Raffone, L.-C. Lin, J. C. Grossman, G. Cicero, *J. Phys. Chem. C* **2020**, *124*, 1438.
[42] F. Raffone, G. Cicero, *ACS Appl. Mater. Interfaces* **2018**, *10*, 7512.
[43] F. Raffone, F. Savazzi, G. Cicero, *J. Phys. Chem. Lett.* **2019**, *10*, 7492.
[44] F. Raffone, F. Savazzi, G. Cicero, *Phys. Chem. Chem. Phys.* **2021**, *23*, 11831.
[45] L.-C. Lin, J. C. Grossman, *Nat. Commun.* **2015**, *6*, 8335.
[46] J. Wang, R. M. Wolf, J. W. Caldwell, P. A. Kollman, D. A. Case, *J. Comput. Chem.* **2004**, *25*, 1157.
[47] K. G. Sprenger, V. W. Jaeger, J. Pfaendtner, *J. Phys. Chem. B* **2015**, *119*, 5882.
[48] G. M. J. Barca, C. Bertoni, L. Carrington, D. Datta, N. De Silva, J. E. Deustua, D. G. Fedorov, J. R. Gour, A. O. Gunina, E. Guidez, T. Harville, S. Irle, J. Ivanic, K. Kowalski, S. S. Leang, H. Li, W. Li, J. J. Lutz, I. Magoulas, J. Mato, V. Mironov, H. Nakata, B. Q. Pham, P. Piecuch, D. Poole, S. R. Pruitt, A. P. Rendell, L. B. Roskop, K. Ruedenberg, T. Sattasathuchana, et al, *J. Chem. Phys.* **2020**, *152*, 154102.
[49] C. I. Bayly, P. Cieplak, W. D. Cornell, P. A. Kollman, *J. Phys. Chem.* **1993**, *97*, 10269.
[50] I. Urrutia, *J. Chem. Phys.* **2011**, *135*, 024511.
[51] N. Takenaka, H. Sakai, Y. Suzuki, P. Uppula, M. Nagaoka, *J. Phys. Chem.* **2015**, *119*, 5582.